Author Manuscript

Author Manuscript

Author Manuscript

Author Manuscript

HHS Public Access

Author manuscript

Mol Cancer Ther. Author manuscript; available in PMC 2025 September 28.

Published in final edited form as:

Mol Cancer Ther. 2025 October 01; 24(10): 1640–1652. doi:10.1158/1535-7163.MCT-24-0873.

Co-Targeting BCL-xL with MCL-1 Induces Lethal Mitochondrial Dysfunction in Diffuse Mesothelioma

Yuan Xu[1], **Cristian G. Medina**[1], **Deborah R. Surman**[2], **Lacey E. Dobrolecki**[3], **Monica Vilchis**[1], **Maheshwari Ramineni**[4], **Susan G. Hilsenbeck**[3], **Yanming Li**[5,6], **Naren Li**[1], **Siqi Wu**[1], **Jaylon C. Aggison**[1], **Xi Chen**[7], **Yi Zhu**[7], **Ying H. Shen**[5,6], **R. Taylor Ripley**[1]

[1]David J. Sugarbaker Division of Thoracic Surgery, Michael E. DeBakey Department of Surgery and the Dan L Duncan Comprehensive Cancer Center, Baylor College of Medicine, Houston, TX, USA.

[2]Michael E. DeBakey Department of Surgery, Baylor College of Medicine, Houston, Texas.

[3]Lester and Sue Smith Breast Center, Baylor College of Medicine, Houston, TX, USA

[4]Department of Pathology and Immunology, Baylor College of Medicine, Houston, TX, USA

[5]Division of Cardiothoracic Surgery, Michael E. DeBakey Department of Surgery, Baylor College of Medicine, Houston, TX, USA

[6]Department of Cardiovascular Surgery, The Texas Heart Institute, Houston, TX, USA

[7]Children's Nutrition Research Center, Department of Pediatrics, Baylor College of Medicine, Houston, TX, USA

Abstract

Diffuse mesothelioma (DM) is a rare but highly aggressive and treatment resistant neoplasm with low survival rates. Effective therapeutic strategies are limited, and resistance to treatment is a major obstacle. Myeloid Cell Leukemia (MCL)-1 and B-cell leukemia (BCL)-xL are anti-apoptotic B-cell lymphoma 2 (Bcl-2) family proteins that block cell-intrinsic apoptosis through interactions on the mitochondrial outer membrane which contribute to therapeutic resistance.

We investigated whether B-cell homology domain (BH)-3 profiles were consistent between intra-patient fresh tumor sample, patient-derived cells (PDC), and patient-derived xenografts (PDX) by BH3 profiling; we observed striking consistency which enabled cross model comparisons. Next, we co-targeted BCL-xl and MCL-1 and noted that the combination synergistically reduced cell viability and increased apoptosis. Mechanistically, BCL-xL inhibition affected the cells through both the canonical and the emerging non-canonical apoptotic pathways. BCL-xL induced

Corresponding Author: R. Taylor Ripley, M.D., Meyer DeBakey Chair of Investigative Surgery, David J. Sugarbaker Division of Thoracic Surgery, Michael E. DeBakey Department of Surgery, Baylor College of Medicine, Houston, TX 77030, R.Taylor.Ripley@bcm.edu.

Authors' contributions

Y. X. and C. M.: Conceptualization, experiments, data curation, formal analysis, investigation, methodology, writing original draft, writing review, and editing. L.D., M. V., D. S., M.R., S.G.H., X.C., SQ W., YM L.: Data curation, formal analysis, methodology, writing review, and editing. Y. Z., H.Y. S, M. TL.: Resources, supervision, validation, investigation. RT.R.: Conceptualization, resources, funding acquisition, formal analysis, supervision, methodology, project administration, writing review, and editing

The authors declare no competing financial interests

Author Manuscript Author Manuscript Author Manuscript Author Manuscript

mitochondrial depolarization which resulted in MCL-1 cellular dependency rendering cells highly sensitive to MCL-1 inhibition. Next, we co-targeted BCL-xL and MCL-1 in vivo which induced synthetic lethality in PDX models within hours, implying that this approach is not a safe strategy for clinical development. However, targeting MCL-1, which exerts its anti-apoptotic activity without non-apoptotic on-target effects, decreased the mitochondrial threshold for apoptosis and enhanced chemosensitivity without toxicity in PDX models. Our findings suggest that targeting the mitochondria via MCL-1 enhances the efficacy of chemotherapy but co-targeting two proteins in the Bcl-2 pathways results in synergistic lethality. These results will help define a safe clinical strategy to utilize Bcl-2 targeted therapy to undermine therapeutic resistance in patients with DM.

Introduction

Diffuse mesothelioma (DM) arises from neoplastic transformation of mesothelial cells lining the pleural cavities and has 5-year overall survival (OS) under 10% [1]. The chemotherapeutic agents, cisplatin and pemetrexed, were United States Food and Drug Administration (FDA)-approved based on a median OS benefit from 9.3 to 12.1 months in 2004.[1] Alternative therapies have minimally impacted survival until 2021 with the landmark trial, CHECKMATE 743, of immune checkpoint inhibitors (ICI).[2] Despite some improvements with systemic chemotherapy or immunotherapy, responses only occur in a subset of patients and resistance is common.

Cell-intrinsic apoptosis, in part, occurs through the mitochondria via the balance of B-cell lymphoma 2 (Bcl-2) family of proteins.[3, 4] Targeting anti-apoptotic Bcl-2 proteins to undermine apoptotic resistance led to a class of small molecule inhibitors known as BH3 mimetics [3]. BH3 mimetics directly target the pro-survival Bcl-2 proteins to sensitize cells to cell death by mitochondrial outer membrane permeabilization (MOMP) [5, 6]. Our previous work showed that DM and esophageal adenocarcinoma (EAC) resist apoptosis through the upregulation of Myeloid Cell Leukemia (MCL)-1; moreover, targeting MCL-1 changed the threshold for apoptosis which enhanced sensitivity to chemotherapy [7, 8]. The anti-apoptotic Bcl-2 proteins have redundant functions; therefore, targeting one protein may upregulate other non-targeted anti-apoptotic Bcl-2 proteins to ensure tumor cell survival. Therefore, co-targeting MCL-1 with BCL-xL is a logical strategy to prevent their redundant functions[9, 10]. Several pharmaceutical companies are currently developing Bcl-2 homology-3 (BH3) mimetics for clinical trials; the Food and Drug Administration (FDA) has approved the first BH-3 mimetic, Venetoclax, an oral Bcl-2 inhibitor to treat chronic lymphocytic leukemia (CLL) and acute myeloid leukemia (AML), [11] a major obstacle associated with these strategies is on-target, dose-limiting toxicity. [12, 13] Therefore, evaluation of mechanisms of co-targeting these proteins is critically important to ensure safe introduction into clinical trials.

BH3 profiling is a live-cell functional bioassay that identifies cellular dependence on individual anti-apoptotic proteins and predicts cellular response to chemotherapy agent and identifies which Bcl-2 proteins are responsible for resistance to apoptosis.[7, 14] The pro- and anti-apoptotic Bcl-2 proteins that regulate MOMP interact with one another at the hydrophobic BH3 domains. BH3 profiling measures the relative interactions of these

Author Manuscript Author Manuscript Author Manuscript Author Manuscript

proteins to determine whether a tumor cell is near the threshold to activate apoptosis ('priming').[14, 15] which predict response to chemotherapy and resistance to targeted therapy in both clinical samples and cell culture [16]. We previously performed BH3 profiling directly on fresh patient tumors of EAC and DM and identified proteins responsible for resistance [7]. Although BH3 profiling is a predictive tool for assessing mitochondrial apoptotic sensitivity, it has not yet undergone sufficient large-scale clinical studies to verify its reliability and predictive power for drug response to determine therapy for patients. Validation of BH3 profiling in patient samples to rapidly assess drug sensitivity is significant to enable clinically feasible timeframes as compared to cell culture or mouse models.

In this study, we examined whether co-targeting MCL-1 and BCL-xL is a safe therapeutic strategy. We expect that BH3 profiling in fresh tumor will serve as a live-cell, predictive bioassay to identify which patient's tumors will respond to BH3 mimetics. Additionally, we expect to establish a safe strategy to introduce BH3 mimetics into clinical trials. Our findings will provide insights into the mechanisms of synergistic effects of targeting Bcl-2 proteins on canonical and non-canonical apoptotic pathways with the goal of undermining therapeutic resistance.

Materials and Methods

Cell culture and Regents

Cell lines H28 and H2452 were purchased from American Type Culture Collection. All cell lines were authenticated yearly with human leukocyte antigen (HLA) analysis and tested for mycoplasma contamination every six months. Cells were cultured in RPMI (ThermoFisher) supplemented with 10% fetal calf serum and 1% penicillin/streptomycin (Gibco). BCL-2 inhibitor, ABT199, was purchased from Apexbio, MCL-1 inhibitor, AZD5991[17], and BCL-xL inhibitor, A11554639[18] were purchased from MCE, and cisplatin was purchased from APP Pharmaceuticals. All regents detail information specified in Table S1.

Primary cells

Mesothelioma tumor specimens were obtained from patients at Baylor College of Medicine and Affiliated Hospitals with Institutional Review Board approval (IRB: H46562), and informed written consent was obtained from each participant. Patients' information specified in Table S2. Tumor samples were obtained by biopsy or surgical resection then minced and dissociated using the human tumor dissociation kit (Miltenyi Biotec). Samples were either incubated at 37 degrees while gently rocking for one hour or dissociated using the gentleMACS system following the manufacturer's protocol. After dissociation, the suspension was filtered through a 70-um cell strainer (BD Falcon) and washed with PBS.

BH3 Profiling

Intracellular BH3 profiling has been previously described in detail.[14, 19] Single cells processing of solid tumors were performed by manually cutting into multiple pieces then digesting by gentleMACS Dissociator (Miltenyi Biotec). After generating single cells, for BH3 profiling, primary cells were first stained with viability dye, LIVE/DEAD™ Fixable Aqua (Thermo Fisher), washed, then incubated with FcR blocking reagent and

Author Manuscript Author Manuscript Author Manuscript Author Manuscript

surface stained with PE anti-human Podoplanin (D2–40) antibody and common leukocyte antigen CD45 antibody. All regents detail information specified in Table S1. Peptide and controls are mixed at 2X desired concentration in MEB2 buffer + 20 μg/ml digitonin (Sigma) and 50 μl of this combination is added per well in a 96 well, non-binding plate. (Supplementary Materials and Methods). The cells, in 50 μl MEB2, are added and incubated with the peptides for one hour at room temperature then fixed. Following neutralization, Anti-Cytochrome C antibody (Biolegend) is added at a 1:2000 final antibody dilution. Staining is performed at 4 C overnight. Viable D2–40 positive and CD45 negative cells were analyzed by multiparameter flow cytometry (Attune NxT, Invitrogen). Retained cytochrome C is measured, and percent cytochrome C release is calculated from the MFI of the cytochrome C stain normalized to that of a well containing 25 μM alamethicin, which serves as 100% release, positive control. For dynamic BH3 profiling (DBP), digested tumor cells were seeded into plates with BH3 mimetics treatment in vitro. After 16h treatments, the cells are collected for subsequent BH3 profiling analysis. “% Delta priming” refers to the percentage change in mitochondrial priming, calculated by comparing the percentage of cytochrome c loss in before and after treatment cells.

Apoptosis analysis

After treatment, cells were stained with Annexin V and PI according to the manufacturer’s instruction. After the cells were incubated at room temperature for 15 min in dark, apoptotic cells were analyzed with flow cytometry (Attune NxT, Invitrogen). Apoptotic cell percentage corresponded to Annexin V(+)/PI(−) and Annexin V(+)/PI(+) cells. Data were analyzed using the FlowJo 10.4.1 software program (Tree Star, USA).

Cell Viability Assay

The half-maximal inhibitory concentration (IC50) curves were generated by plating 3000 cells/well in a 96 well plate (Corning, NY). Cells were treated overnight with ABT199, A1155463, or cisplatin was added the next day at the indicated concentrations. Viability was assessed by CellTiter-Glo 2.0 Reagent (Supplementary Materials and Methods). Synergy scoring was determined using the “inhibition readout” on the online SynergyFinder software (https://synergyfinder.fimm.fi) [20] specified in Supplementary Materials and Methods.

Animal Studies

All animal experiments were performed in accordance with the Guide for the Care and Use of Laboratory Animals and protocols approved by the Institutional Animal Care and Use Committee (IACUC) of Baylor College of Medicine. PDXs were established by Patient-Derived Xenograft and Advanced In Vivo Models (PDX-AIM) core.[21] Fresh PDX tumor fragments were transplanted into the cleared, #4 mammary fat-pad (right abdominal) of female, five-week-old NSG mice (JAX, NOD.Cg-Prkdcscid Il2rgtm1Wjl/SzJ (RRID:BCBC_4611)) and allowed to grow to the study start size of 50 mm^3. The mice were randomized to each treatment groups and were treated with vehicle control, AZD5991, A1155463, AZD5991/A1155463, cisplatin (CDDP), CDDP/AZD5991, A1155364/CDDP, or the combination of three drugs via intraperitoneal injection. The dosage and frequency of drug administration was specified in the figure legends. Body weights and tumor sizes were

Author Manuscript Author Manuscript Author Manuscript Author Manuscript

measured every three days by blinding investigators. Animals were euthanized if 1) tumor volume was ≥ 1500 mm^3; 2) tumor became ulcerated.

Western Blots

Equal amounts of protein were separated by 4–20% SDS-polyacrylamide gel electrophoresis and were transferred to polyvinylidene fluoride (PVDF) membranes (Millipore, Billerica, MA). Membranes were incubated overnight at 4 °C with primary antibodies at the concentrations specified in Table S1. After additional incubation with an anti-immunoglobin horseradish peroxidase-linked Ab for 1 h, the immune complexes were detected by the SuperSignal® West Femto Maximum Sensitivity Substrate (Thermo Fisher Scientific).

Seahorse Extracellular Flux Analysis

Oxygen consumption rates (OCR) and extracellular acidification rates (ECAR) of cells were measured using a Seahorse Bioscience XF96 Extracellular Flux Analyzer (Supplementary Materials and Methods). Seahorse programing consisted of 3-minute baseline measurements with 1-minute intervals which were repeated after each injection. All values were normalized to DNA content of each well to account for growth differences.

JC-1 assays

Mitochondrial membrane potential ($\Delta\psi m$) changes were detected using the mitochondrial membrane potential-sensitive fluorescent dye JC-1 (Thermo Fisher Scientific) following the manufacturer's instructions. After treatments, cells were collected and suspended in PBS at approximately 1×10^6 cells/ml containing JC-1 and the cells incubated at 37 °C, 5% CO_2 for 30 min. After loading, the cells were washed twice with PBS and analyzed by flow cytometry (Attune NxT, Invitrogen).

Mitochondrial ROS detection assay

MitoSOX™ mitochondrial superoxide indicators (Thermo Fisher Scientific) were used to measure mitochondrial superoxide production within the cell according to the manufacturer's protocol. After treatments, cells were collected and suspended in PBS at approximately 1×10^6 cells/ml containing indicators and the cells incubated at 37 °C, 5% CO_2 for 1h, cells were analyzed on FACS flow cytometer (Attune NxT, Invitrogen). Relative fluorescence intensities were analyzed using FlowJo 10.4.1 software (RRID:SCR_008520).

Immunofluorescence staining

Cells were seeded in Millicell EZ SLIDE 4-well glass (Millipore) for immunofluorescence staining according to the protocol. Representative microphotographs were acquired using EVOS M5000 Imaging System. For high-resolution imaging, cells were seeded in ibidi μ-Slide 8 Well high coverslip (Germany) overnight, the ONI Discovery Kit (ONI US, CA) was used for direct stochastic optical reconstruction microscopy (dSTROM) according to the manufacturer's protocol(Supplementary Materials and Methods).

Author Manuscript Author Manuscript Author Manuscript Author Manuscript

Statistical Analysis

Quantitative data were presented as the mean ± SD. The student *t* test was carried out to compare means between two groups. One-way ANOVA followed by the *post hoc* Dunnett test was used to compare means of more than two groups, and a multiple range least significant difference (LSD) was used for intergroup comparisons. For in vivo studies, the tumor growth curves were converted to log2 fold change from baseline and were evaluated using general linear models with random effects to account for mouse within treatment group dependencies. Fold change data at the single time point were simplified to evaluate tumor size changes at a specific time point using repeated-measures analysis of variance (ANOVA) analyses. Results with $P < 0.05$ were considered statistically significant and are indicated by $^{*,\#}$, $P < 0.05$; and **, $^{\#\#}$, $P < 0.01$. All statistical analyses were performed with SPSS 16.0 (RRID:SCR_002865) and Graph pad.

Results

Dynamics BH3 profiling in DM specimens reveals patient-specific responses.

Our previous work established that BH3 profiling can identify cell dependence on different anti-apoptotic proteins in cultured cell lines as well as fresh EAC and DM tumors [7]. To assess translational potential and further verify the predictive role of BH3 profiling in DM patients, we generated patient-derived cell (PDC) and patient-derived xenograft (PDX) models from patient tumor tissue collected at surgery. Four PDCs and one PDX were successfully established. The PDCs had different morphologies, malignant characteristics, cell proliferation rates, colony formation activities, migration, and invasion. Several notable DM makers (PanCK, WT-1, D2–40 and CK5/6)[22] were evaluated in PDCs cells which noted heterogeneity and varity in PDC cell lines (Supplementary Figure S1). After establishing the PDCs and PDX models, we confirmed that the PDC and MPM188 PDX model retained the histological characteristics of the original tumor (Supplementary Figure S2 and Table S3). Next, we performed BH3 profiling on fresh tumor, PDC, and PDX to determine whether BH3 profiles were similar between the models from the same patient (Figure 1A). The binding patterns of BH3 peptides (BIM, BAD, NOXA, MS-1, and HRK) and BH3 mimetics (A1155463, AZD5991, ABT199) to anti-apoptotic proteins (BCL-2, BCL-xL, and MCL-1) were used in the BH3 profiling (Figure. 1B) The BH3 profiles of DM patients showed similar activities in the tumor samples 4 hours after surgery compared to both PDC and PDX models (Figure 1C and Supplementary Figure S3A). For example, one patient strongly responded to MSI BH3 peptides in addition to the ubiquitous sensitizer, BIM, in all models which suggested sensitivity to MCL-1 antagonism (Figure 1C). This prediction was confirmed by noting significant increases in apoptosis with MCL-1 inhibitor, AZD-5991, in combination with cisplatin (CDDP) compared to the BCL-2 inhibitor or BCL-xL inhibitor (Figure 1D and Supplementary Figure S3B). These results show that BH3 profiling is similar across the models and predictive of response to BH3 mimetic treatments.

After verifying the predictive role of *BH3 profiling* in DM patients, we performed *Dynamic BH3 Profiling (DBP)* to evaluate whether BH3 mimetics induced mitochondrial apoptotic priming (decreased the threshold to trigger apoptosis) in DM patients (Figure 1E). DBP generates a ‘delta priming’ which is the comparison of BH3 profiles before and after drug

Author Manuscript Author Manuscript Author Manuscript Author Manuscript

treatment.[23, 24] Increased priming indicates dependence on corresponding anti-apoptotic proteins. We performed DBP in seven DM patients; the heatmap indicated differences in mitochondrial priming between patients. Patients M1207 and MPM196 showed relatively poor priming with BH3 mimetics, whereas patients MPM188 and MPM207 appeared to have a marked response to MCL-1 and BCL-xL inhibition. Furthermore, in all patients treated with BH3 mimetics, we noticed that the MCL-1 sensitizers, NOXA and MS1 peptides, are most responsive when treated with the BCL-xL inhibitor, A1155463. Additionally, when treated with the MCL-1 inhibitor, AZD5991, the peptides, BAD and HRK, were increased which suggests these tumors are now responsive to BCL-xL (Figure 1F). These results suggested that BCL-xL and MCL-1 have functional redundancy in which they play compensatory roles for each other. In other words, when treating MCL-1, BCL-xL increases as a compensatory mechanism to prevent induction of apoptotic pathways.

To further investigate clinical importance of Bcl-2 proteins, we assessed the expression profiles of MCL-1, BCL-xL and BCL-2 in a tissue microarray. High MCL-1 expressions were found in 88 of 94 cases (93%), high combination of MCL-1, BCL-xL and BCL-2 expressions was observed in 19 of 94 cases (20%), and high BCL-xL and MCL-1 were observed in 40 of 94 cases (43%). MCL-1^{high}/BCL-xL^{high} population (63%) is the most common profile in DM (Figure 1G). These results suggest that targeting both MCL-1 and BCL-xL may be a treatment strategy for patients with DM.

Synergistic cell death is induced by the combination of MCL-1 and BCL-xl inhibition in DM cell lines.

Most solid tumors are not sensitive to single-agent treatment with BH3 mimetics.[10, 23, 25–27] We previously reported that S63845(previously used agent), ABT199 (targeting BCL-2), and A1155463 (targeting BCL-xL) had weak activity on EAC and DM cells.[7] We extended these findings to additional DM cell lines as well as DM PDC. As expected, all cells were relatively resistant to single agent AZD5591, A1155463, and ABT199 (Figure 2A). Given that MCL-1 and BCL-xL are co-expressed in DM, we treated the cell lines, H28 and H2452, and PDC to evaluate the cytotoxic activity of AZD5991 in combination with titrated, non-sensitizing concentrations of A1155463. Cell death was observed with A1155463 with IC50 values 60 to 200-fold less than single agents in DM cells (Supplementary Figure S4A). The combination treatment resulted in significant cytotoxicity in insensitive cells with either treatment alone (Figure 2B and Supplementary Figure S4B). With the synergyfinder program, we assessed AZD5991 and A1155463 combinations and observed a distribution that confirmed the predictive, synergistic effects in the region around IC50. These results are based on synergy scores over 10 which is considered synergistic. The most synergistic area was 0.125 μM to 0.5 μM, which showed about 80% inhibition with a score around 30 (Figure 2C and 2D and Supplementary Figure S4C). Based on these results, we chose 0.1 μM as the combination dose for future studies. In our previous work, we found that targeting MCL-1 or BCL-xl with S63845 or A1155463 in combination with the cisplatin (CDDP) significantly increased apoptosis compared to CDDP alone.[7] To determine if redundancy of MCL-1 and BCL-xl reduced the synergistic effects of either agent alone with CDDP, we treated cells with the combination of AZD5991 and A1155463 with CDDP. We observed that targeting both MCL-1 and BCL-xL significantly

Author Manuscript Author Manuscript Author Manuscript Author Manuscript

increased apoptosis with CDDP (Figure 2E and Supplementary Figure S4D). Hence, these data demonstrate that co-targeting BCL-xL and MCL-1 may block the compensatory mechanisms of Bcl-2 anti-apoptotic proteins to synergistically increase apoptosis and enhance chemotherapy response.

MCL-1 inhibition enhances antitumor response of cisplatin in PDX models.

We evaluated AZD5991 and A-1155463 in MPM188 PDX model. First, we performed a tolerance study in non-tumor bearing NSG mice with AZD5991 at 0.5 mg/kg – 10 mg/kg and A1155463 at 0.25 mg/kg – 5 mg/kg. We found that the combination of MCL-1 and BCL-xL at lower doses was well tolerated based on stable body weight (Figure 3A). In contrast, higher doses were lethal within five hours even though the single agents were well tolerated at the same dose.

Next, we performed an efficacy in vivo experiment. Mice bearing MPM188 tumors were randomized into 8 arms with vehicle, full dose (FD) AZD5991, FD A1155463, FD AZD5991 or FD A1155463 with cisplatin, and low dose (LD) with and without CDDP (Figure 3B). FD AZD5591 and FD A1155463 as single agents as well as LD combination of AZD5991 and A1155463 did not result in significant tumor growth inhibition consistent with our in vitro results. In contrast, single-agent FD AZD5991 with CDDP significantly reduced tumor growth. Treatment with FD A1155463 also resulted in significant growth inhibition; however, A1155463 was less effective than AZD5991 (Figure 3C–D and Supplementary Table S4). We confirmed the enhanced efficacy of the single-agent FD AZD5991 with CDDP by the mass of tumors collected on day 78 when the vehicle group reached endpoint; the slight tumor suppression effects observed with the triple combination treatment compared to single-agent treatments are attributable to the low combination doses used, which, while synergistic in vitro, may not reach optimal therapeutic efficacy in vivo at these safety levels (Figure 3E). Moreover, AZD5991 with CDDP significantly increased survival compared to vehicle or single agent treatments (Figure 3F). Importantly, body weight remained constant during the in vivo study period and mice appeared healthy after treatment. These data suggested that MCL-1 inhibition increases mitochondrial priming to enhance the chemosensitivity to CDDP in DM.

We performed DBP on harvested mouse tumors and compared each treatment arm to control to identify anti-apoptotic dependency changes. The PDX tumors treated with AZD5991 and CDDP had the most growth inhibition which was consistent with the greatest change in the DBP. In contrast, the DBP showed almost no priming in LD combination group which is consistent with a lack of tumor response. AZD5991 or CDDP showed significantly increased response to MS1, BAD and NOXA BH3 peptide indicating an increased dependency to MCL-1. While an increase in HRK BH3 peptide suggests that MCL-1 antagonism also drives BCL-xL dependency (Figure 3G). Our results are consistent with prior reports that DBP measures early changes in apoptotic signaling which occur before frank apoptosis.[28] These data confirm that BCL-xL and MCL-1 have compensatory roles in anti-tumor effects, antagonizing one results in increased dependence on the other.

Author Manuscript Author Manuscript Author Manuscript Author Manuscript

Co-targeting MCL-1 and BCL-xL synergistically increase cell death through the intrinsic mitochondrial apoptotic pathway.

We evaluated whether co-targeting BCL-xL and MCL-1 synergistically increases cell death via the mitochondrial apoptotic pathways. We knocked down MCL-1 and BCL-xL (shMCL-1 and shBCL-xL) to determine whether these knockdowns phenocopied pharmacological inhibition. First, H28 and H2452 cells did not survive double knockdown of MCL-1 and BCL-xL. Interestingly, the protein expression of MCL-1 was significantly elevated in shBCL-xL H28 and H2452 cells, whereas shMCL-1 had no effect on BCL-xL expression. BCL-2 expression did not have a consistent pattern in either H28 and H2452 cell lines with MCL-1 and BCL-xL knockdowns (Figure 4A). Our previous study found that mesothelioma has a lower dependence on Bcl-2 for survival and less sensitive to its targeted inhibition ABT199.[7] Therefore, in this study, we did not explore the ABT199 efficacy in mesothelioma. Next, we treated shMCL-1 cells with the BCL-xL inhibitor, A1155463, and shBCL-xl cells with MCL-1 inhibitor, AZD5991. shMCL-1 sensitized the cells to A1155463; similarly, shBCL-xL sensitized the cells to AZD5991 (Figure 4B). Significantly increased apoptosis was observed in shMCL-1 or shBCL-xL cells with the drug targeting the other protein (Figure 4C). These results are consistent with the synergistic effects of dual pharmacological inhibition of MCL-1 and BCL-xL.

MCL-1 and BCL-xL exert antiapoptotic activity by inhibiting the effector proteins of MOMP called BAX and BAK [3]. To verify on-target engagement of MOMP when co-targeting MCL-1 and BCL-xL, we knocked down BAX and BAK ($DKD^{bax/bak}$) (Figure 4D). The $DKD^{bax/bak}$ cells were significantly more resistant to the AZD5991 and A1155463 with 60% of shCTL cells exhibiting apoptosis compared to less than 20% of $DKD^{bax/bak}$ (Figure 4F). We repeated the experiments in PDCs (MPM188 and MPM193) and noted similar findings that blocking MOMP by $DKD^{bax/bak}$ prevented synergistic cell death when co-targeting MCL-1 and BCL-xL (Supplementary Figure S5).

BCL-xL inhibition induced mitochondrial damage and dysfunction.

MCL-1 and BCL-xL maintain mitochondrial integrity and dynamics.[29–32] To investigate whether MCL-1 and BCL-xL play contributing roles in mitochondrial integrity and dynamics during treatment-induced cell death, we assessed mitochondrial changes in H28 and H2452 cells. To assess morphology, we performed direct stochastic optical reconstruction microscopy (dSTORM) to observe mitochondria ultrastructural changes at super resolution.[33] Cells were labeled with mitochondrial marker, TOM20. We observed reticulated and elongated mitochondria in shCTL and shMCL-1 cells. In contrast, the mitochodria were fragmented and almost exclusively perinuclear in shBCL-xL cells (Figure 5A). Similarity, A1155463 induced markedly perinuclear clustering of mitochondria unlike AZD5991. Additionally, H28 and H2452 cells with LD AZD5991 and A1155463 combination showed the presence of punctate-like mitochondria throughout the cytoplasm (Figure 5B). Mitochondrial freagmentation results in loss of fusion or increase in fission. However, we did not observe consistent changes of mitochondrial fission (Drp1, FIS1) and fusion (MFN1, MFN2) proteins after the inhibition of MCL-1 or BCL-xL in vitro or vivo (Supplementary Figure S6). These results suggest that the synergistic effects of MCL-1 and BCL-xL on tumor cell death are not mediated via fusion or fission.

Author Manuscript Author Manuscript Author Manuscript Author Manuscript

Given that mitochondria clustering coinciding with nuclear fragmentation is potentially a distinct feature of cells with dysfunctional mitochondria [34, 35], additionally, given that we observed that targeting BCL-xL led to marked perinuclear clustering of mitochondrial, we investigated the effects of BCL-xL and MCL-1 on the mitochondrial metabolic status by measuring oxidative phosphorylation (OXPHOS). Seahorse data showed that shBCL-xL resulted in significant decreases in ATP production, basal resperiation, and maximal respiration compared with shMCL-1 and shCTL in H2452 cells (Figure 5C). Similarily, we observed lower decreased oxygen consumption rates (OCR) in cells with BCL-xL inhibitor, A1155463 (Figure 5D). OXPHOS deficiency reduces mitochondrial membrane potential ($\Delta\psi m$) with concomitant increases in reactive oxygen species (mtROS).[36, 37] We observed that inhibition of BCL-xL decreased mitochondrial membrane potential by JC-1 (Figure 5E). Similar changes were observed with pharmacological inhibition of BCL-xL (Figure 5F). Meanwhile, we found that genetic or pharmacological inhibition of BCL-xL induced mitochondrial superoxide production compared with MCL-1 inhibition (Figure 5G and 5H). These observations suggest that BCL-xL inhibition impaired mitochondrial respiration, increased mtROS production, and enhanced mitochondrial membrane damage leading to mitochondrial dysfunction, while MCL-1 inhibition did not show similar toxic effects on the mitochondria.

BCL-xL inhibition induced MCL-1 accumulation in mitochondria.

Given that shBCL-xL significantly increases MCL-1 levels (Figure 4A) and co-targeting BCL-xL and MCL-1 synergistically increases cell death (Figure 2B), [30] we hypothesized that cell death with BCL-xL inhibition was protected by the increase in MCL-1 protein expression on the mitochondrial membrane and, thus, these cells were particularly vulnerable to MCL-1 inhibition. We investigated the localization of MCL-1 in shBCL-xl cells by immunofluorescence and observed MCL-1 accumulation localized to the mitochondria in shBCL-xL cells (Figure 6A). We confirmed by mitochondrial and cytosolic protein extraction (Figure 6B). Similarly, mitochondrial accumulation of MCL-1 was observed in H28 and H2452 cells when treated with BCL-xL inhibitor, A1155463, MCL-1 was overexpressed after AZD5991 treatments, and the majority MCL-1 protein increases in cytosolic fraction with AZD5991 treatments (Figure 6C and 6D), due to AZD5991 blocked MCL-1 ubiquitination via enhanced deubiquitinating to increase MCL-1 protein stability. [38] Additionally, in H28 and H2452 cells treated with LD AZD5991 and A1155463, highly fragmented and dispersed mitochondria with lower levels of MCL-1 were noted which confirms that the mitochondria are highly damaged by the combination treatment. This mitochondrial impairment likely contributes to the synergistic effects on cell death.

Discussion

BH3 profiling is a functional predictive biomarker for BH3 mimetic treatment. [6, 23, 28, 39] However, BH3 profiling to rapidly and directly assess the drug responsiveness in patients' fresh primary tumors is limited. In this project, we evaluated whether BH3 profiles are consistent from the same patient samples in fresh tumor after 4 hours, in PDC after 3 months in culture, and in PDX developed over 1.5 years. Importantly, we observed similar BH3 profiles in all models. For example, we noted that similarities in response to BAD

Author Manuscript Author Manuscript Author Manuscript Author Manuscript

and MS1 peptides in fresh tumor as well as PDX. The adaptation during long-term ex vivo culture alters drug sensitivity compared to fresh tumor; our results suggest that BH3 profiles which measure real-time, mitochondrial protein interactions remain stable over time. These findings enable mechanistic studies on long-term PDC and PDX models to further investigate results derived from fresh tumor. Ultimately, the goal is to perform DBP as a predictive assay of drug response within days of biopsy to guide precision-based treatment decisions in each patient. To date, DBP has not been performed to change clinical decisions. Our results will help validate that findings in long-term models may be applicable to results obtained within hours of biopsy.

BCL-xL and MCL-1 are important in DM as noted in our cell line and TMA data.[40, 41] We previously demonstrated that inhibiting either BCL-xL or MCL-1 alone had limited impact on cell death;[7] we verified that targeting MCL-1 or BCL-xL as single agents in PDX models had minimal efficacy consistent with others' work [41, 42]. Given that MCL-1 and BCL-xL exhibit functional redundancy, we evaluated whether dual inhibition is a more effective strategy. Recently, many groups showed that co-targeting BCL-xL and MCL-1 is highly effective in a variety of tumors.[9, 43] Ryan et al. performed a drug screen in ten tissue types to a combination of selective BCL-2, BCL-xL, and MCL-1 inhibitors and discovered that most cell lines displayed synergistic dependence on BCL-xL and MCL-1.[26] Similarly, co-targeting MCL-1 and BCL-xL resulted in reduced cell viability of cells from head and neck squamous cell carcinoma[44]. BCL-xL antagonism was reported to sensitize DM cell lines to MCL-1 inhibition.[23, 40] Others report that RNAi against MCL-1 and BCL-xL induce DM cell death.[45] Our data also showed that combinational treatment with A1155463 and AZD5991 induced rapid and almost 100% cell death in DM cells lines and PDC. However, toxicity may limit clinical implementation. We found that the combination of MCL-1 and BCL-xL inhibitors were rapidly lethal in mice within 5 hours. Other groups have observed the same effects.[23] We decreased the dose by a factor of 10 and noted that all mice tolerated the treatment but had almost no anti-tumor efficacy. Other groups have shown that the dosing schedule of navitoclax and S63845 can overcome toxicity and maintain anti-tumor efficacy.[6, 9] Another group tried to avoid the off-target effects of BCL-xL inhibition in the human hematopoietic system and of MCL-1 inhibition in cardiac toxicity by using very low doses of S63845 and A-1331852.[10] Regardless, titrating to a safe therapeutic window will be challenging and may limit clinical development.

MCL-1 and BCL-xL have functions beyond apoptosis. MCL-1 regulates the mitochondrial inner membrane mediated fission enhancing its ablity to antagonize cell death.[46, 47] BCL-xL prevents loss of outer membrane integrity to maintain mitochondrial metabolite exchanges by preventing membrane hyperpolarization and mitochondrial swelling in response to a diverse set of stimuli.[31, 48] We found that BCL-xL inhibition induced mitochondrial morphology changes and perinuclear clustering. These phenotypes were not observed when targeting MCL-1 which indicates that mitochondrial homeostasis is less dependent on MCL-1 and that BCL-xL has potential functions other than the canonical apoptosis. These findings are supported based on inconsistent changes of mitochodniral fission (Drp1, FIS1) and fusion (MFN1, MFN2) proteins with MCL-1 inhibition. MCL-1 maintains mitochondrial homeostasis by interactions with DRP-1 and OPA1 which are essential regulators of mitochondrial morphology and dynamics.[46, 49] Therefore, blocking

Author Manuscript Author Manuscript Author Manuscript Author Manuscript

MCL-1 may result in the inability to alter mitochodrial dynamics. Alternatively, MCL-1 is localized to distinct mitochondrial sub-compartments that alter mitochondrial activity and integrity [30, 50]. Regardless, MCL-1 exerts its anti-apoptotic activity on the outer mitochondrial membrane (OMM) where it antagonizes BAX and BAK activation which is critical to chemosensitization.[51]

Our data shows that high levels of MCL-1 are present on the mitochondria after BCL-xL inhibition which is likely required to maintain mitochondrial integrity. This integrity is lost with inhibition of both MCL-1 and BCL-xL which may explain the lethality of this approach. Moreover, we found that BCL-xL inhibition impaired mitochondrial respiration and decreased mitochondrial membrane potential. Blocking BCL-xL likely enables opening permeability transition pores on the mitochondrial membrane by increasing Ca^{2+} accumulation in the mitochondrial matrix.[48] Based on other reports and our data showing that knockdown of BCL-xL significantly increases MCL-1 levels in mitochondria, we speculate that BCL-xL inhibition through its canonical apoptotic and emerging non-apoptotic roles impairs mitochondrial dysfunction by directly inducing depolarization and energy loss resulting in increased MCL-1 dependency. Our results reveal mitochondrial fragmentation with BCL-xL inhibition support this mechanism.

Collectively, we found that BH3 profiling served as a live-cell, predictive bioassay to identify patient responses to treatments, which has high potential for near-term translation to the clinic. Furthermore, we found that dual inhibition of MCL-1 and BCL-xL is synthetic lethality and not a safe treatment strategy. However, the FDA placed the clinical hold on Mcl-1 inhibitor AZD5991 (NCT03218683) and AMG 397 (NCT03465540) following cardiac toxicity. [52] In addition to the on-target thrombocytopenia from BCL-xL, our study shows that BCL-xL inhibition induces mitochondrial dysfunction through non-apoptotic on-target effects. However, MCL-1 inhibition appears safe and efficacious when combined with standard chemotherapy but may not be tolerated with another Bcl-2 inhibitor. These findings may lead to the re-emergence of MCL-1-targeting agents in clinic use.

Supplementary Material

Refer to Web version on PubMed Central for supplementary material.

Acknowledgements

This work was supported by the NIH R03 Award (R03 CA252685–01), the NIH R21 Award (R21 CA256466), NIH R37 Award (R37 CA289419), NIH R01 Award (MPI-R01 CA290173); Michael E. DeBakey Department of Surgery Faculty Research Award, and Roderick D. MacDonald Research Fund at Baylor St. Luke's Medical Center.

This project was supported by the Cytometry and Cell Sorting Core at Baylor College of Medicine (BCM) with funding from the CPRIT Core Facility Support Award (CPRIT-RP180672), the NIH (CA125123 and RR024574) and the assistance of Joel M. Sederstrom; Pathology and Histology Core (HTAP) at BCM with funding from the Dan L. Duncan Comprehensive Cancer Center NIH grant (P30 Cancer Center Support Grant (NCI-CA125123)); Patient-Derived Xenograft Core at BCM with funding from P30 Cancer Center Support Grant NCI-CA125123, CPRIT Core Facilities Support Grant RP220646; Mouse Metabolism and Phenotyping Core at BCM with funding from NIH UM1HG006348, NIH R01DK114356, NIH R01HL130249. This work was supported by Dan L. Duncan Comprehensive Cancer Center grant (CA P30125123).

Author Manuscript Author Manuscript Author Manuscript Author Manuscript

Disclosures

RTR: Federally funded grants: R37(R01 NCI Merit Award) CA289419; R01 (MPI) CA290173; R21 CA256466; R03 CA252685; U01 CA214195; U24 2U24OH009077. Society Grants: DeGregorio Family Foundation for Gastric Esophageal Malignancies; AATS Foundation: Surgical Investigator Program. Clinical Trial Support: Investigator-Initiated Trial funded by AstraZeneca; Industry trials in lung cancer funded by Genentech. National Leadership Positions: Vice President of the Meso Foundation; Steering Committee for National Mesothelioma Virtual Databank; Steering Committee for IASLC Mesothelioma Staging Project.

Data Availability

Data related to sensitive patient information has been anonymized to protect privacy and the data generated in this study is available upon reasonable request to the corresponding author.

Reference

1. Vogelzang NJ, et al. , Phase III Study of Pemetrexed in Combination With Cisplatin Versus Cisplatin Alone in Patients With Malignant Pleural Mesothelioma. J Clin Oncol, 2023. 41(12): p. 2125–2133. [PubMed: 37068377]
2. Baas P, et al. , First-line nivolumab plus ipilimumab in unresectable malignant pleural mesothelioma (CheckMate 743): a multicentre, randomised, open-label, phase 3 trial. Lancet, 2021. 397(10272): p. 375–386. [PubMed: 33485464]
3. Tait SW and Green DR, Mitochondria and cell death: outer membrane permeabilization and beyond. Nat Rev Mol Cell Biol, 2010. 11(9): p. 621–32. [PubMed: 20683470]
4. Potter DS and Letai A, To Prime, or Not to Prime: That Is the Question. Cold Spring Harb Symp Quant Biol, 2016. 81: p. 131–140. [PubMed: 27811212]
5. Sarchen V, et al. , Pediatric multicellular tumor spheroid models illustrate a therapeutic potential by combining BH3 mimetics with Natural Killer (NK) cell-based immunotherapy. Cell Death Discov, 2022. 8(1): p. 11. [PubMed: 35013156]
6. Bhatt S, et al. , Reduced Mitochondrial Apoptotic Priming Drives Resistance to BH3 Mimetics in Acute Myeloid Leukemia. Cancer Cell, 2020. 38(6): p. 872–890 e6. [PubMed: 33217342]
7. Surman DR, et al. , Therapeutic Synergy in Esophageal Cancer and Mesothelioma is Predicted by Dynamic BH3 Profiling. Mol Cancer Ther, 2021.
8. Xu Y, et al. , Bile acid-induced “Minority MOMP” promotes esophageal carcinogenesis while maintaining apoptotic resistance via Mcl-1. Oncogene, 2020. 39(4): p. 877–890. [PubMed: 31570787]
9. Mukherjee N, et al. , MCL1 inhibitors S63845/MIK665 plus Navitoclax synergistically kill difficult-to-treat melanoma cells. Cell Death Dis, 2020. 11(6): p. 443. [PubMed: 32513939]
10. Abdul Rahman SF, et al. , Dual inhibition of anti-apoptotic proteins BCL-XL and MCL-1 enhances cytotoxicity of Nasopharyngeal carcinoma cells. Discov Oncol, 2022. 13(1): p. 9. [PubMed: 35201512]
11. Del Poeta G, et al. , Venetoclax: Bcl-2 inhibition for the treatment of chronic lymphocytic leukemia. Drugs Today (Barc), 2016. 52(4): p. 249–60. [PubMed: 27252989]
12. Cleary JM, et al. , A phase I clinical trial of navitoclax, a targeted high-affinity Bcl-2 family inhibitor, in combination with gemcitabine in patients with solid tumors. Invest New Drugs, 2014. 32(5): p. 937–45. [PubMed: 24916770]
13. Yuda J, et al. , Selective MCL-1 inhibitor ABBV-467 is efficacious in tumor models but is associated with cardiac troponin increases in patients. Commun Med (Lond), 2023. 3(1): p. 154. [PubMed: 37880389]
14. Ryan J, et al. , iBH3: simple, fixable BH3 profiling to determine apoptotic priming in primary tissue by flow cytometry. Biol Chem, 2016. 397(7): p. 671–8. [PubMed: 26910743]
15. Del Gaizo Moore V and Letai A, BH3 profiling--measuring integrated function of the mitochondrial apoptotic pathway to predict cell fate decisions. Cancer Lett, 2013. 332(2): p. 202–5. [PubMed: 22230093]

Author Manuscript Author Manuscript Author Manuscript Author Manuscript

16. Ni Chonghaile T, et al. , Pretreatment mitochondrial priming correlates with clinical response to cytotoxic chemotherapy. Science, 2011. 334(6059): p. 1129–33. [PubMed: 22033517]
17. Tron AE, et al. , Discovery of Mcl-1-specific inhibitor AZD5991 and preclinical activity in multiple myeloma and acute myeloid leukemia. Nat Commun, 2018. 9(1): p. 5341. [PubMed: 30559424]
18. Tao ZF, et al. , Discovery of a Potent and Selective BCL-XL Inhibitor with in Vivo Activity. ACS Med Chem Lett, 2014. 5(10): p. 1088–93. [PubMed: 25313317]
19. Ryan J and Letai A, BH3 profiling in whole cells by fluorimeter or FACS. Methods, 2013. 61(2): p. 156–64. [PubMed: 23607990]
20. Ianevski A, et al. , SynergyFinder: a web application for analyzing drug combination dose-response matrix data. Bioinformatics, 2020. 36(8): p. 2645. [PubMed: 32118251]
21. Lv X, et al. , Orthotopic Transplantation of Breast Tumors as Preclinical Models for Breast Cancer. J Vis Exp, 2020(159).
22. Husain AN, et al. , Guidelines for Pathologic Diagnosis of Malignant Mesothelioma 2017 Update of the Consensus Statement From the International Mesothelioma Interest Group. Arch Pathol Lab Med, 2018. 142(1): p. 89–108. [PubMed: 28686500]
23. Potter DS, et al. , Dynamic BH3 profiling identifies pro-apoptotic drug combinations for the treatment of malignant pleural mesothelioma. Nat Commun, 2023. 14(1): p. 2897. [PubMed: 37210412]
24. Olesinski EA and Bhatt S, Dynamic BH3 profiling method for rapid identification of active therapy in BH3 mimetics resistant xenograft mouse models. STAR Protoc, 2021. 2(2): p. 100461. [PubMed: 34027474]
25. Xu D, et al. , Malignant pleural mesothelioma co-opts BCL-X(L) and autophagy to escape apoptosis. Cell Death Dis, 2021. 12(4): p. 406. [PubMed: 33859162]
26. Soderquist RS, et al. , Systematic mapping of BCL-2 gene dependencies in cancer reveals molecular determinants of BH3 mimetic sensitivity. Nat Commun, 2018. 9(1): p. 3513. [PubMed: 30158527]
27. Campbell KJ, et al. , Breast cancer dependence on MCL-1 is due to its canonical anti-apoptotic function. Cell Death Differ, 2021. 28(9): p. 2589–2600. [PubMed: 33785871]
28. Potter DS, et al. , Dynamic BH3 profiling identifies active BH3 mimetic combinations in non-small cell lung cancer. Cell Death Dis, 2021. 12(8): p. 741. [PubMed: 34315868]
29. Anilkumar U, et al. , MCL-1(Matrix) maintains neuronal survival by enhancing mitochondrial integrity and bioenergetic capacity under stress conditions. Cell Death Dis, 2020. 11(5): p. 321. [PubMed: 32371858]
30. Perciavalle RM, et al. , Anti-apoptotic MCL-1 localizes to the mitochondrial matrix and couples mitochondrial fusion to respiration. Nat Cell Biol, 2012. 14(6): p. 575–83. [PubMed: 22544066]
31. Vander Heiden MG, et al. , Bcl-xL regulates the membrane potential and volume homeostasis of mitochondria. Cell, 1997. 91(5): p. 627–37. [PubMed: 9393856]
32. Nguyen TTM, et al. , Mitochondrial Bcl-xL promotes brain synaptogenesis by controlling non-lethal caspase activation. iScience, 2023. 26(5): p. 106674. [PubMed: 37182099]
33. Durel B, Kervrann C, and Bertolin G, Quantitative dSTORM super-resolution microscopy localizes Aurora kinase A/AURKA in the mitochondrial matrix. Biol Cell, 2021. 113(11): p. 458–473. [PubMed: 34463964]
34. Dewitt DA, et al. , Peri-nuclear clustering of mitochondria is triggered during aluminum maltolate induced apoptosis. J Alzheimers Dis, 2006. 9(2): p. 195–205.
35. Mori MP, et al. , Mitochondrial respiration reduces exposure of the nucleus to oxygen. J Biol Chem, 2023. 299(3): p. 103018. [PubMed: 36796514]
36. Sturm G, et al. , OxPhos defects cause hypermetabolism and reduce lifespan in cells and in patients with mitochondrial diseases. Commun Biol, 2023. 6(1): p. 22. [PubMed: 36635485]
37. Tao S, et al. , Mitochondrial reactive oxygen species promote mitochondrial damage in high glucose-induced dysfunction and apoptosis of human dental pulp cells. J Dent Sci, 2024. 19(1): p. 292–302. [PubMed: 38303803]

Author Manuscript Author Manuscript Author Manuscript Author Manuscript

38. Tantawy SI, et al. , Mechanisms of MCL-1 Protein Stability Induced by MCL-1 Antagonists in B-Cell Malignancies. Clin Cancer Res, 2023. 29(2): p. 446–457. [PubMed: 36346691]
39. Montero J, et al. , Drug-induced death signaling strategy rapidly predicts cancer response to chemotherapy. Cell, 2015. 160(5): p. 977–989. [PubMed: 25723171]
40. Arulananda S, et al. , BCL-XL is an actionable target for treatment of malignant pleural mesothelioma. Cell Death Discov, 2020. 6(1): p. 114. [PubMed: 33298868]
41. Arulananda S, et al. , A novel BH3-mimetic, AZD0466, targeting BCL-XL and BCL-2 is effective in pre-clinical models of malignant pleural mesothelioma. Cell Death Discov, 2021. 7(1): p. 122. [PubMed: 34050131]
42. Jackson MR, et al. , Mesothelioma Cells Depend on the Antiapoptotic Protein Bcl-xL for Survival and Are Sensitized to Ionizing Radiation by BH3-Mimetics. Int J Radiat Oncol Biol Phys, 2020. 106(4): p. 867–877. [PubMed: 31786278]
43. Abdul Rahman SF, et al. , Co-inhibition of BCL-XL and MCL-1 with selective BCL-2 family inhibitors enhances cytotoxicity of cervical cancer cell lines. Biochem Biophys Rep, 2020. 22: p. 100756. [PubMed: 32346617]
44. Heimer S, et al. , Hypertonicity counteracts MCL-1 and renders BCL-XL a synthetic lethal target in head and neck cancer. FEBS J, 2021. 288(6): p. 1822–1838. [PubMed: 32710568]
45. Varin E, et al. , Downregulation of Bcl-xL and Mcl-1 is sufficient to induce cell death in mesothelioma cells highly refractory to conventional chemotherapy. Carcinogenesis, 2010. 31(6): p. 984–93. [PubMed: 20142415]
46. Moyzis AG, et al. , Mcl-1-mediated mitochondrial fission protects against stress but impairs cardiac adaptation to exercise. J Mol Cell Cardiol, 2020. 146: p. 109–120. [PubMed: 32717194]
47. Widden H and Placzek WJ, The multiple mechanisms of MCL1 in the regulation of cell fate. Commun Biol, 2021. 4(1): p. 1029. [PubMed: 34475520]
48. Tornero D, Posadas I, and Cena V, Bcl-x(L) blocks a mitochondrial inner membrane channel and prevents Ca2+ overload-mediated cell death. PLoS One, 2011. 6(6): p. e20423. [PubMed: 21674052]
49. Morciano G, et al. , Mcl-1 involvement in mitochondrial dynamics is associated with apoptotic cell death. Mol Biol Cell, 2016. 27(1): p. 20–34. [PubMed: 26538029]
50. Lacombe A and Scorrano L, The interplay between mitochondrial dynamics and autophagy: From a key homeostatic mechanism to a driver of pathology. Semin Cell Dev Biol, 2024. 161–162: p. 1–19.
51. Huang CR and Yang-Yen HF, The fast-mobility isoform of mouse Mcl-1 is a mitochondrial matrix-localized protein with attenuated anti-apoptotic activity. FEBS Lett, 2010. 584(15): p. 3323–30. [PubMed: 20627101]
52. Tantawy SI, et al. , Targeting MCL-1 protein to treat cancer: opportunities and challenges. Front Oncol, 2023. 13: p. 1226289. [PubMed: 37601693]

Author Manuscript Author Manuscript Author Manuscript Author Manuscript

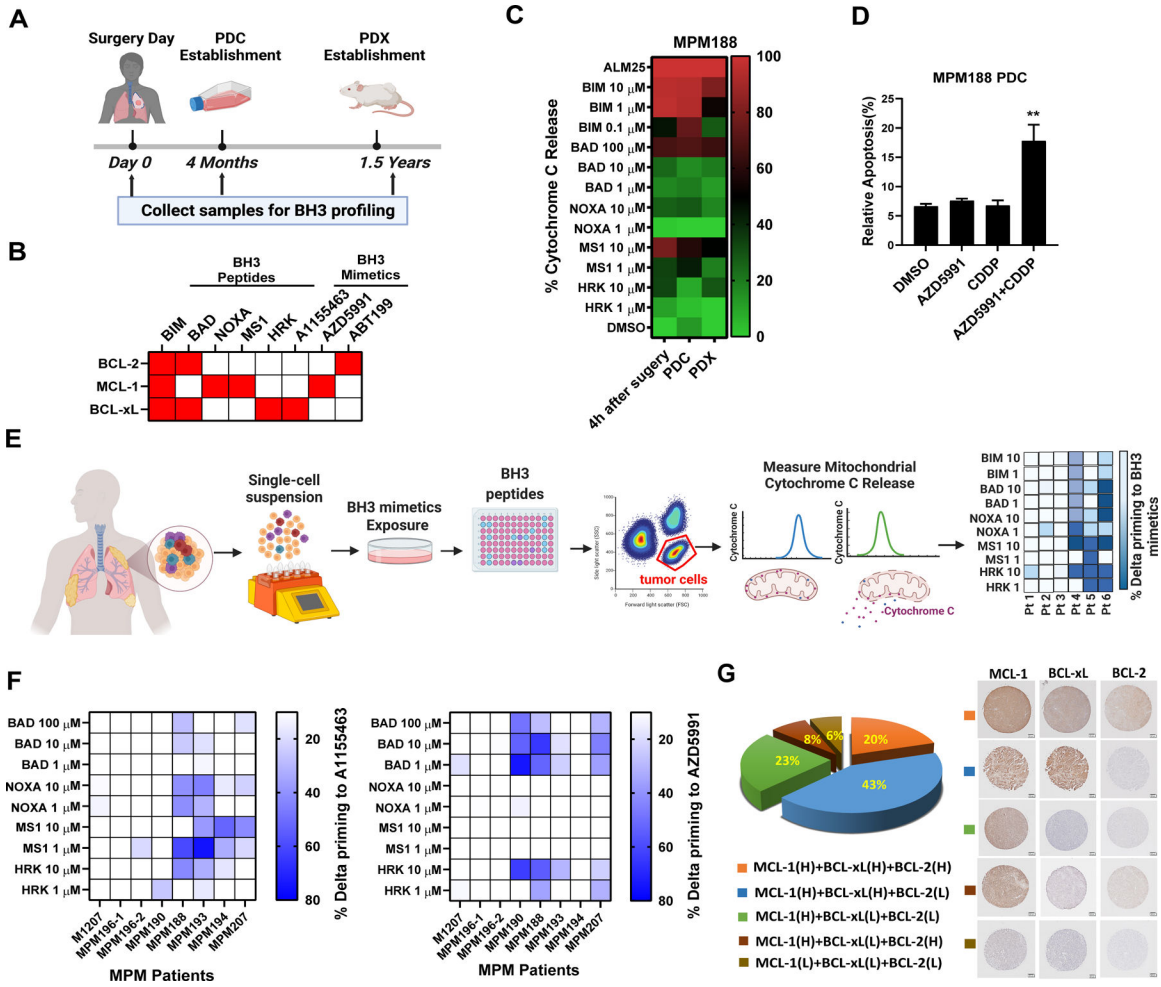

Figure 1. Dynamic BH3 profiling in DM specimens reveals patient-specific responses.

A. Timeline of BH3 profiling in fresh DM patients' sample, DM derived cells (PDCs) and xenografts (PDXs). Created with BioRender.com. **B.** Interaction map for BH3 peptides and BH3 mimetics with BCL-2 family proteins. Red indicates high-affinity binding and white indicates low-affinity binding. **C.** Heatmap showing BH3 profiling in MPM188 patient samples 4 h compared to PDC and PDX when exposed to the indicated peptides. Data was normalized to DMSO (as negative control) and alamethicin (ALM25, as positive control). **D.** After pre-treatment with 1.0 μM AZD5991 for 24 h, the apoptotic ratio in cells at 48 h after treatment with CDDP were measured by annexin V flow cytometry; cells positive for annexin V staining were counted as apoptotic cells (** $p < 0.01$ for treatment versus DMSO). **E.** The workflow for measuring BH3 mimetics-induced priming using DBP on primary DM patient samples. Created with BioRender.com. **F.** Heatmap of mitochondrial priming of fresh samples with 1.0 μM AZD5991 or A1155463 treatment for 16 h. **G.** The expression profiles of MCL-1, BCL-xL, and BCL-2 in each case are shown as a percentage of all 50 cases. (H) or (L) means high or low expression, respectively. Representative images of immunohistochemical expressions of MCL-1, BCL-xL, and BCL-2 in TMA from DM patients.

Author Manuscript Author Manuscript Author Manuscript Author Manuscript

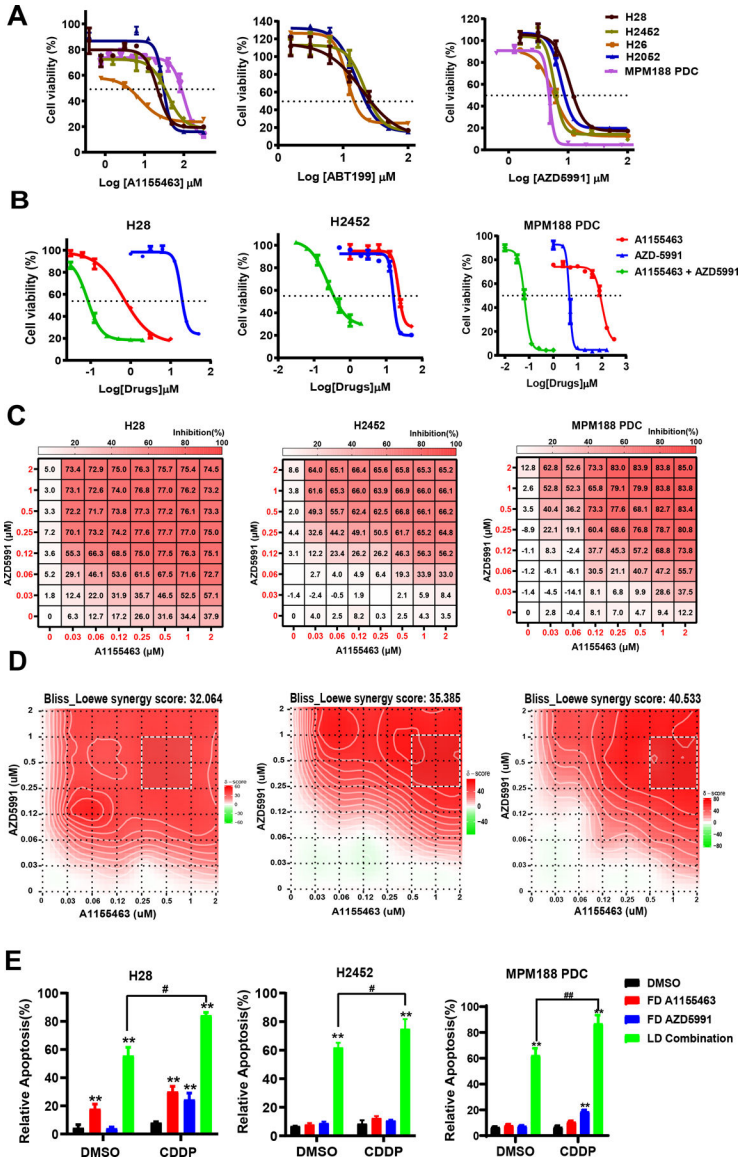

Figure 2. Synergistic cell death is induced by the MCL-1 inhibitor, AZD5991, and BCL-xL inhibitor, A1155463, in DM cell lines.

A. Single agent activity of BH3-mimetics in DM cell lines after 48 h of treatment. The IC50 values of AZD5991, A1155463, and ABT199 were calculated. Data is presented as mean ± SD of four technical replicates from three independent experiments. **B.** Cell death was assessed upon exposure of DM cell lines to increasing concentrations of AZD5991 and/or A1155463 for 48 h. Data are presented as mean ± SD of three technical replicates from three independent experiments. **C.** The heatmaps showing does-response matrix analyses based on cell death with the MCL-1 inhibitor, AZD5991, and BCL-xL inhibitor, A1155463. **D.** Visualization of the calculated 2D synergy maps for the cell viability assay from the SynergyFinder Bliss_Loewe independence model combinatorial analysis. Red regions represent synergy and green regions represent antagonism. **E.** After pre-treatment with full does (FD) 1.0 μM AZD5991 or FD 1.0 μM A1155463, and the combination of low does (LD) 0.1 μM AZD5991 and LD 0.1 μM A1155463 for 24 h, the apoptotic ratio in cells at 48

h after treatment with CDDP were measured by annexin V flow cytometry; cells positive for annexin V staining were counted as apoptotic cells (** $p < 0.01$ for treatment versus DMSO; #$p < 0.05$ for combination treatment versus A1155463 and AZD5991 co-treatment).

Author Manuscript Author Manuscript Author Manuscript Author Manuscript

Author Manuscript Author Manuscript Author Manuscript Author Manuscript

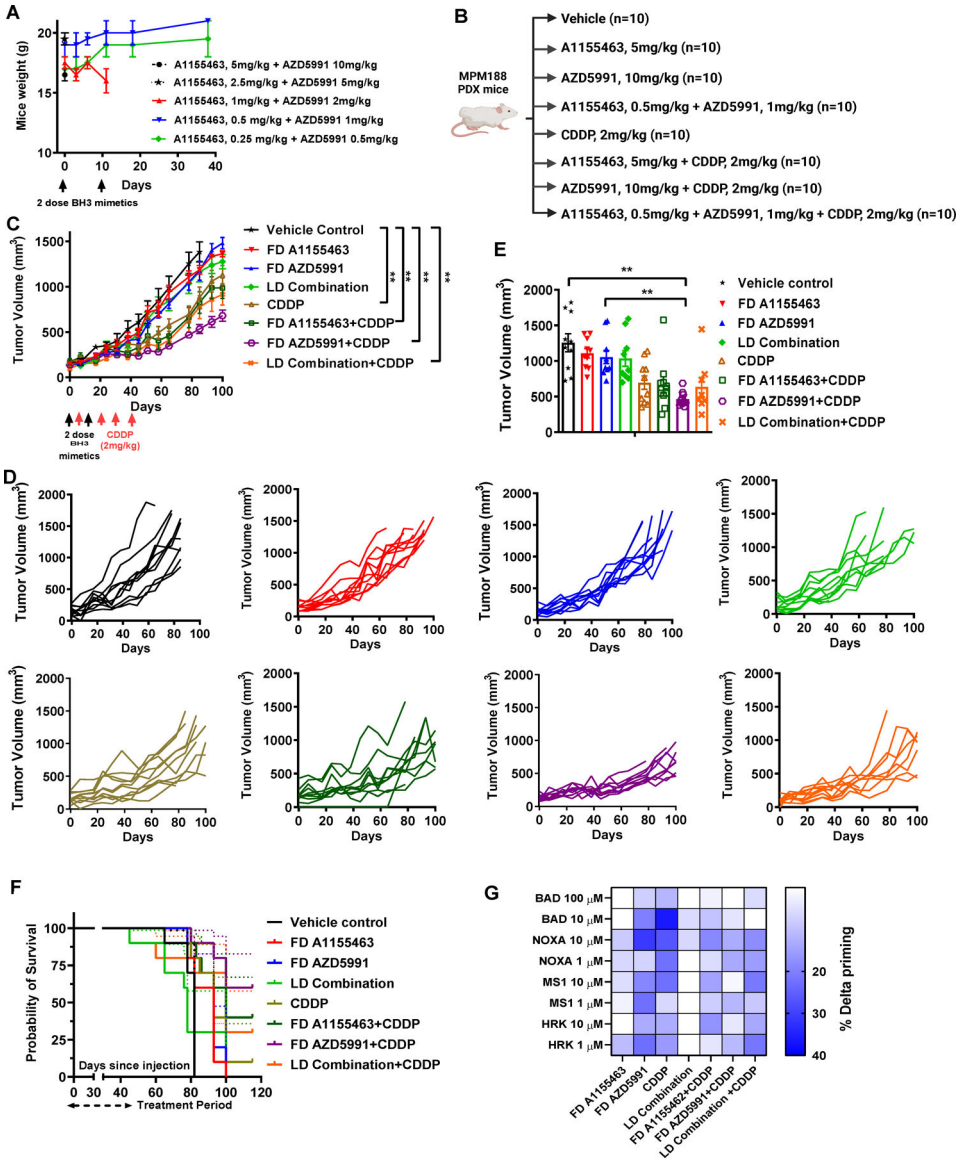

Figure 3. MCL-1 inhibitor AZD5991 enhances antitumor response of cisplatin in MPM188 PDX model.

A. Changes of mouse body weight upon treatment with different combinational concentrations of AZD5991 and A1155463. **B.** Groups of mice for the experiment. Once the tumor volume reached between 50 and 100 mm^3, the mice were randomized to each treatment or control group and were treated with vehicle control, full does (FD) AZD5991 (10mg/kg), FD A1155463 (5mg/kg), low does (LD) AZD5991 (1mg/kg) and A1155463 (0.5mg/kg), cisplatin (CDDP) (2mg/kg), the combination of FD AZD55991 and CDDP, combination of FD A1155364 and CDDP, or the combination of LD AZD5991 and LD A1155463 with CDDP via intraperitoneal injection. **C.** Cumulative graph of mean tumor size (mm^2) per group. (** $p < 0.01$ for treatments versus vehicle control; **D.** Tumor size (mm^2) of individual mice in each group from experiment described in (B). **E.** Tumor masses on Day 78 (the day that vehicle group reached endpoint). Each point is the mass of an individual tumor with the bar indicating the mean ± SD (n =10). (** p <

Author Manuscript Author Manuscript Author Manuscript Author Manuscript

0.01 for combination treatment versus single AZD5991 treatment or vehicle control). **F.** Kaplan–Meier survival curves with log-rank analysis of mice treated with different groups, with relevant vehicle controls. The survival endpoint was when tumors reached 1500 mm^3 as dictated by the ethics approval associated with this experiment. **G.** Heatmap of mitochondrial priming was generated by comparison of BH3 profiles of PDX samples from vehicle control groups between each treatment arms.

Author Manuscript Author Manuscript Author Manuscript Author Manuscript

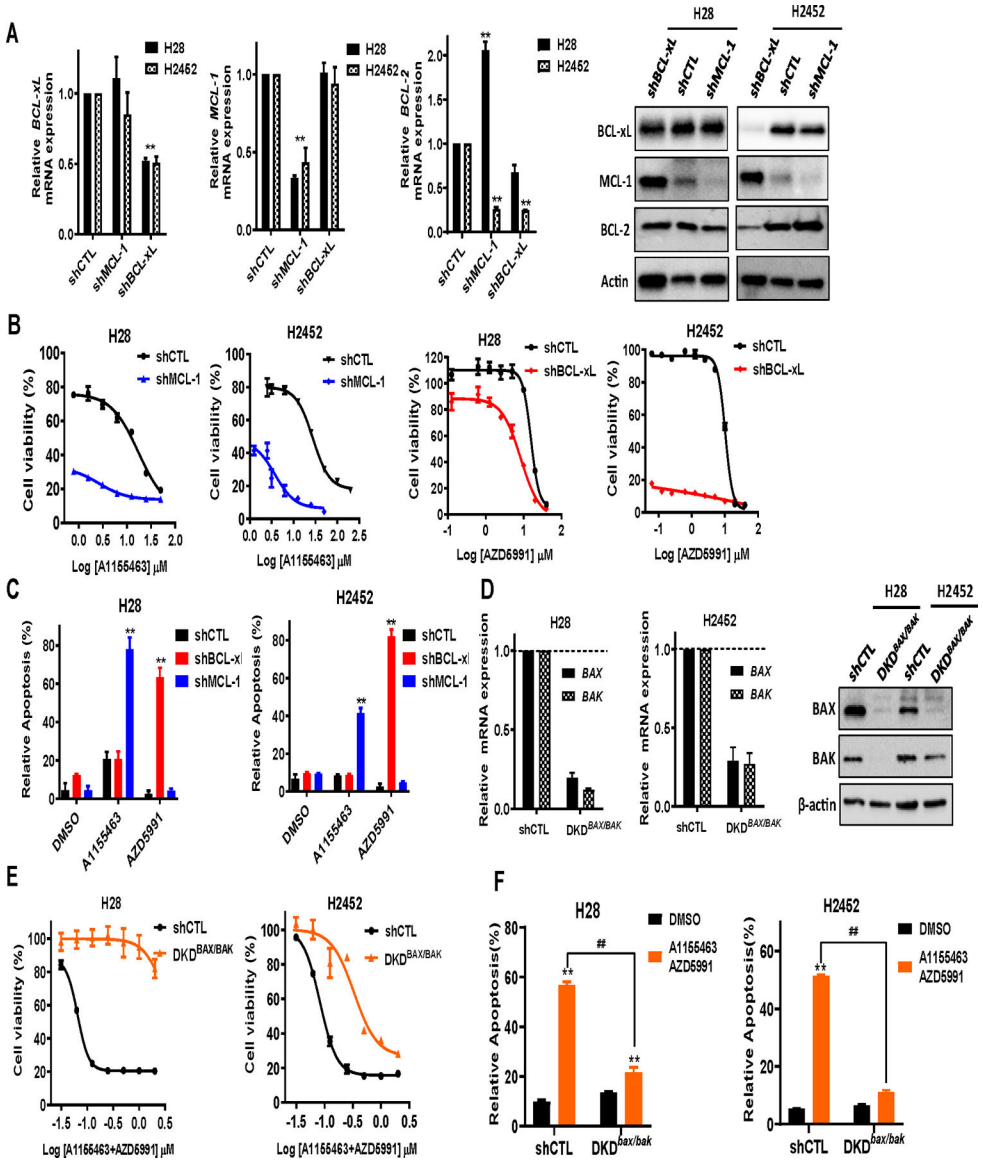

Figure 4. Co-targeting MCL-1 and BCL-xL synergistically increase cell death through the intrinsic mitochondrial apoptotic pathway in DM cell lines.

A. Stable knock-down of MCL-1 (shMCL-1), BCL-xL (shBCL-xL), or scrambled control (shCTL) were generated in H28 and H2452 cells by transfecting short-hairpin RNA lentiviruses. The mRNA and protein levels of MCL-1, BCL-xL and Bcl-2 were analyzed by qRT-PCR analysis and western blot. **B.** Cell viability at 48 h in shCTL, shMCL-1, and shBCL-xL cell lines treated with either AZD5991 or A1155436 alone. The IC50 values of AZD5991 and A1155463 were determined in different condition cells. Data are mean ± SD of four technical replicates from three independent experiments. **C.** After pre-treatment with 1.0 μM FD AZD5991 or 1.0 μM FD A1155463, the apoptotic ratio in shCTL, shMCL-1, and shBCL-xL cells were measured by annexin V flow cytometry; cells positive for annexin V staining were counted as apoptotic cells (** $p < 0.01$ for treatment versus DMSO in respective cells). **D.** Stable double knock-down of Bax and Bak ($DKD^{bax/bak}$) or scrambled control (shCTL) were generated in H28 and H2452 cells by transfecting short-hairpin RNA

Author Manuscript Author Manuscript Author Manuscript Author Manuscript

lentiviruses. The mRNA and protein levels of Bax and Bak were analyzed by qRT-PCR analysis and western blot. **E.** Cell viability at 48 h in shCTL and DKD$^{Bax/Bak}$ cell lines when treated with the combination of AZD5991 and A1155463. The IC50 values of AZD5991 and A1155463 were determined in different conditions. Data are mean ± SD of four technical replicates from three independent experiments. **F.** After pre-treatment with the combination of LD AZD5991 and A1155463 for 24 h, the apoptotic ratio in shCTL and DKD$^{Bax/Bak}$ cells were measured by annexin V flow cytometry; cells positive for annexin V staining were counted as apoptotic cells (** $p < 0.01$ for treatment versus DMSO, $^{\#\#}$ $p < 0.01$ for DKD$^{Bax/Bak}$ versus scrambled control).

Author Manuscript
Author Manuscript
Author Manuscript
Author Manuscript

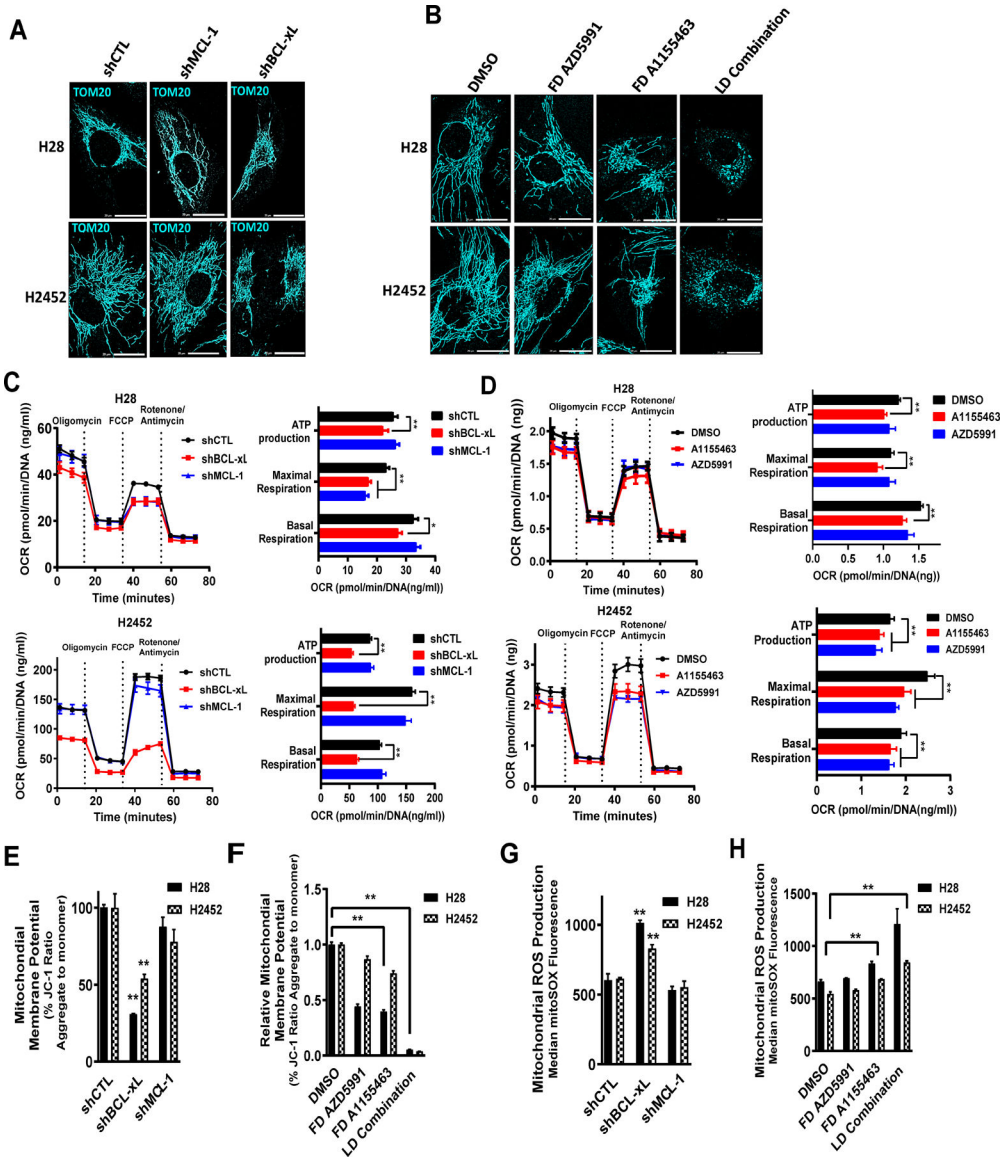

Figure 5. BCL-xL inhibition induced mitochondrial damage and dysfunction in DM cell lines.

A. Representative **s**uper-resolution imaging of mitochondria labeled with TOM20 in shCTL, shMCL-1, and shBCL-xL cell lines. Scale bar: 20 μm. **B.** Representative super-resolution imaging of mitochondria labeled with TOM20 in H28 and H2452 cells with FD AZD5991, FD A1155463, and LD combination of AZD5991 and A1155463 treatments for 24 h. Scale bar: 20 μm. **C.** Oxygen consumption rate (OCR) was measured with sequential injections of oligomycin, FCCP, and rotenone/antimycin at the time points indicated in shCTL, shMCL-1, and shBCL-xL in H28 and H2452 cell lines. Basal Respiratory capacity, maximal respiration, and ATP production were calculated as described in Supplementary Materials and Methods section. **D.** After treatment with FD AZD5991, FD A1155463, or the combination of LD AZD5991 and A1155463 for 24 h, the OCR was measured with sequential injections of oligomycin, FCCP, and rotenone/antimycin at the time points indicated in H28 and H2452 cell lines. **E.** Analysis of mitochondrial membrane potentials

Author Manuscript Author Manuscript Author Manuscript Author Manuscript

(ΔΨm) using flow cytometry with JC-1 dye in shCTL, shMCL-1, and shBCL-xL in H28 and H2452 cell lines. Loss of ΔΨm was demonstrated by the change in JC-1 fluorescence from red (JC-1 aggregates) to green (JC-1 monomers) represented as ratio of JC-1 red to green fluorescence in different conditional cells (**P<0.01compared with indicated control groups). **F.** After treatment with FD AZD5991, FD A1155463, or the combination of LD AZD5991 and A1155463 for 24 h, mitochondrial membrane potentials (ΔΨm) were measured using flow cytometry with JC-1 dye in H28 and H2452 cell lines (**P<0.01compared with indicated control groups). **G.** Mitochondrial ROS concentrations were measured using MitoSOX™ Red reagent by flow cytometry with the median of fluorescence ± SD analyzed using FlowJo software in shCTL, shMCL-1, and shBCL-xL in H28 and H2452 cell lines. (**P<0.01compared with indicated control groups). **H.** After treatment with FD AZD5991, FD A1155463, or the combination of LD AZD5991 and A1155463 for 24 h, mitochondrial ROS concentrations was measured using MitoSOX™ Red reagent by flow cytometry with the median of fluorescence ± SD analyzed using FlowJo software in conditional H28 and H2452 cells (**P<0.01compared with indicated control groups).

Author Manuscript Author Manuscript Author Manuscript Author Manuscript

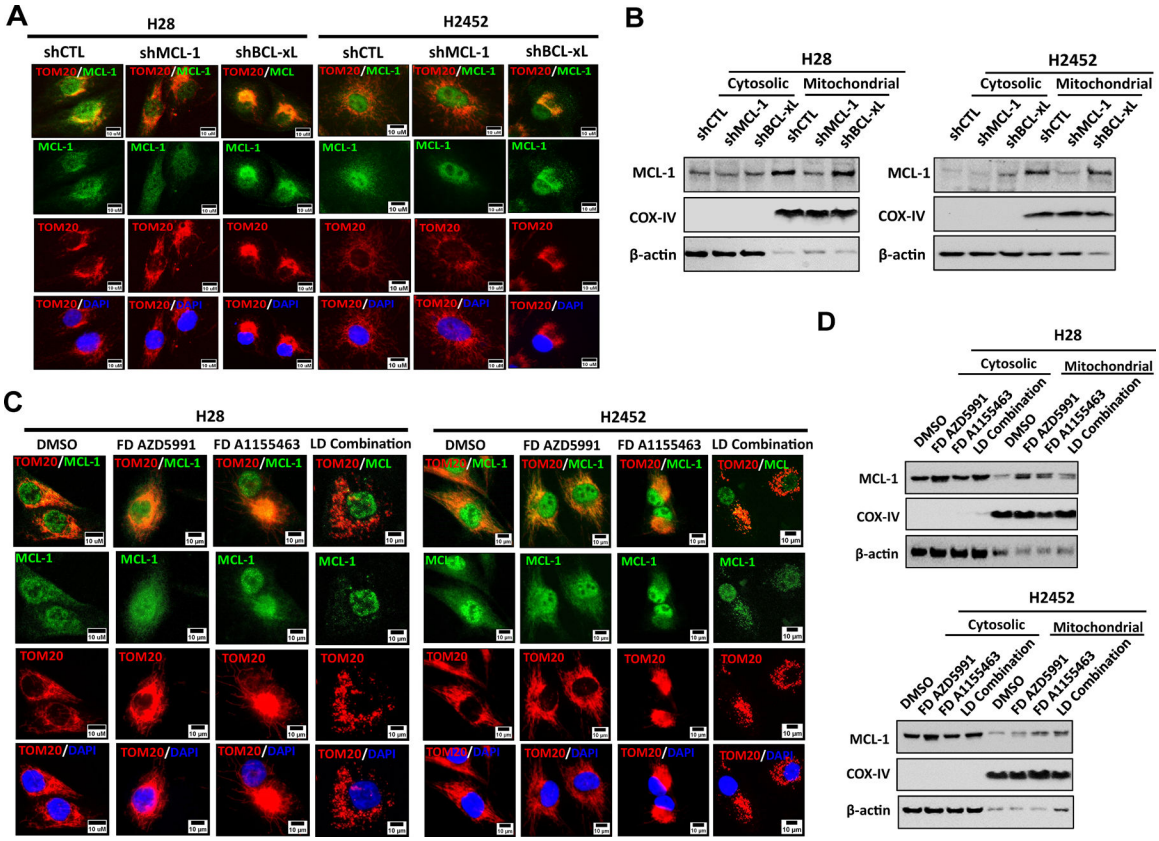

Figure 6. BCL-xL inhibition induced MCL-1 translocation to mitochondria in DM cells.

A. Colocalization between mitochondria and MCL-1 was assessed in shCTL, shMCL-1, and shBCL-xL H28 and H2452 cell lines by immunofluorescence staining of TOM20 (Red), MCL-1 (Green), and the nucleus by DAPI (Blue). Scale bar: 10μm. **B.** Immunoblots for MCL-1 were performed on the mitochondrial and cytosolic fractions in shCTL, shMCL-1, and shBCL-xL H28 and H2452 cell lines. Separation of mitochondria and cytosol was controlled using COX IV and β-actin, respectively. **C.** H28 and H2452 cells were used to assess the mitochondrial integrity and colocalization with MCL-1 after FD AZD5991, FD A1155463, or LD combination of AZD5991 and A1155463 for 24 h by immunofluorescence staining of TOM20 (Red), MCL-1 (Green), and the nucleus by DAPI (Blue). Scale bar: 10μm. **D.** H28 and H2452 cells were treated with FD AZD5991, FD A1155463, or LD combination of AZD5991 and A1155463 for 24 h. Immunoblots for MCL-1 were performed on the mitochondrial and cytosolic fractions in different conditions treated H28 and H2452 cells. Separation of mitochondria and cytosol was controlled using COX IV and β-actin, respectively.